minerals

MDPI

Article

Synchrotron Micro-X-ray Diffraction in Transmission Geometry: A New Approach to Study Polychrome Stratigraphies in Cultural Heritage

Giulia Morabito [1], Nicoletta Marinoni [1], Giorgio Bais [2], Marco Cantaluppi [1], Alessandra Botteon [3], Chiara Colombo [3], G. Diego Gatta [1,*], Maurizio Polentarutti [2], Marco Realini [3] and Elena Possenti [3]

[1] Dipartimento di Scienze della Terra "Ardito Desio", Università degli Studi di Milano, Via Botticelli 23, 20133 Milano, Italy; giulia.morabito@unimi.it (G.M.); nicoletta.marinoni@unimi.it (N.M.); marco.cantaluppi@unimi.it (M.C.)

[2] ELETTRA Sincrotrone Trieste S.C.p.A., Strada Statale 14 - km 163,5 in Area Science Park, 34149 Basovizza, Italy; giorgio.bais@elettra.eu (G.B.); maurizio.polentarutti@elettra.eu (M.P.)

[3] Istituto di Scienze del Patrimonio Culturale (ISPC), Consiglio Nazionale delle Ricerche (CNR), Via R. Cozzi 53, 20125 Milano, Italy; alessandra.botteon@cnr.it (A.B.); chiara.colombo@cnr.it (C.C.); marco.realini@cnr.it (M.R.); elena.possenti@cnr.it (E.P.)

* Correspondence: diego.gatta@unimi.it; Tel.: +39-020315607

Abstract: In cultural heritage, paint stratigraphies are complex systems typically consisting of various paint layers with fine crystalline phases mixed with coarse pigment and filler grains. This complexity poses significant challenges for X-ray diffraction (XRD) analysis. In this work, we employed synchrotron radiation micro-X-ray diffraction in transmission geometry (SR-μTXRD) with linear mapping to develop a novel approach for studying the crystalline phases (pigments and fillers) in mock-up paint stratigraphies. A targeted approach was followed for qualitative, quantitative, and microstructural analysis, combining signals from micrometric crystallites and coarse single crystals as well as from randomly oriented and iso-oriented crystalline phases. This allows for identifying, localizing, and quantifying these phases even in low fractions and distinguishes the same phases across different layers with varying grain sizes or spatial orientations. Critical analysis of 2D XRD patterns, coupled with full-profile fitting performed by the Rietveld method, provides insights into material preparation (e.g., grinding), painting technique (e.g., color palette, use of fillers, brushing), and crystallo-chemical modifications over time. This analytical approach, integrating spatially resolved investigation with high-quality phase characterization, enhances the potential of specific XRD methodologies for a 2D investigation of multi-phase materials in cultural heritage, even without dedicated micro-mapping techniques.

Keywords: paint stratigraphy; synchrotron radiation micro-X-ray diffraction in transmission geometry; Rietveld method; XRD mapping; pigments; fillers

Citation: Morabito, G.; Marinoni, N.; Bais, G.; Cantaluppi, M.; Botteon, A.; Colombo, C.; Gatta, G.D.; Polentarutti, M.; Realini, M.; Possenti, E. Synchrotron Micro-X-ray Diffraction in Transmission Geometry: A New Approach to Study Polychrome Stratigraphies in Cultural Heritage. *Minerals* **2024**, *14*, 866. https://doi.org/10.3390/min14090866

Academic Editors: Marco Benvenuti, Rosarosa Manca and Lucilla Fabrizi

Received: 20 June 2024
Revised: 17 August 2024
Accepted: 20 August 2024
Published: 25 August 2024

1. Introduction

Paint stratigraphies are of great interest in the fields of heritage science and conservation science. Information about their composition and micro-structure, both at and below the surface, enables an unveiling of the painting techniques, the employed materials, and the variations that occurred over time [1,2]. The awareness that the materials of cultural heritage (CH) objects change inexorably with time in response to their composition (i.e., chemical reactions that take place within paint layers and below the surface) or to their interaction with the surrounding environment (i.e., chemical reactions that take place at the interface between the paint surface and the air) leads research increasingly towards modern approaches to study the composition and the external and sub-subsurface microstructure of paint stratigraphies [3–5]. The analytical characterization of the chemistry, mineralogy, and spatial distribution of crystalline phases in paint layers also provides a substantial

contribution to explore the state of conservation of a work of art and its conservation history, also investigating the presence of decay phases and/or restoration products as well as distinguishing between genuine and counterfeit artifacts [1,2,4,6,7].

In many cases, an exhaustive analytical investigation of paint stratigraphies is not a straightforward task. In general, they represent very complex systems, characterized by compositional and microstructural heterogeneity from the macro- to the microscopic scale. They are multi-layered systems of micrometric layers with irregular thickness and consist of a mixture of compounds, including organic and inorganic substances in crystalline and amorphous phases [2–8]. Each paint layer is, moreover, generally composed of several pigments or fillers, and these particles may be both heterogeneously distributed within the paint layers and characterized by very different grain sizes, resulting in the coexistence of very fine-grained particles in a mixture with coarser ones. Such a compositional and microstructural complexity makes their characterization an analytical challenge that sets the conditions to develop advanced multi-analytical approaches.

Working with fragments from works of art commonly imposes the necessity to investigate very small samples (as in the case of the paint stratigraphies) and to identify mineral phases in very low weight fractions, whose detection and quantification are analytically very challenging. In this complex scenario, the use of analytical laboratory-scale sources is crucial to obtain preliminary information about the stratigraphy, but often a similar approach faces several limitations due to the complexity of the materials and the instrumental detection limits. Therefore, a multi-analytical characterization requires, in some cases, the use of unconventional sources, such as synchrotron radiation (SR) [9–11].

In recent years, synchrotron-based X-ray techniques have provided valuable insights into the study and characterization of pigments, micrometric paint samples, or entire paintings thanks to the use of pencil X-ray beams [12,13]. Specifically, the choice of using SR-based techniques to study these complex materials is due to their unique instrumental capabilities and source properties, such as brightness, small beam size, and energy tunability in a broad spectral range [14,15]. These properties have led to the development of a wide range of X-ray-based analytical techniques [16–19], offering structural characterization, high elemental sensitivity, chemical specificity, and three-dimensional imaging with spatial resolution down to the nanometric length scale, requiring a very low mass sample. These characteristics are particularly beneficial for the study of highly heterogeneous and complex samples from CH, such as those from paintings, as demonstrated by some of the most recent SR X-ray multi-analytical studies, carried out on small micro-fragments of masterpieces by Cimabue, Pablo Picasso, and Rembrandt [16–19].

Focusing on X-ray diffraction (XRD), different geometries can be used for XRD analysis: grazing incidence, reflectance, and transmission (in capillary or thin section) [20–23]. The XRD analysis carried out in transmitting geometry with SR and a micro-sized X-ray beam (SR-μTXRD) has turned out to be, in recent years, an extremely powerful analytical approach in CH studies, and many articles have been published based on the study of pigments, alteration products, and conservation treatments [1,9,16]. The transmission mode geometry, performed on a thin section of paint stratigraphies, allows the investigation of the samples providing crystallo-chemical information of the crystalline phases in polycrystalline materials with a spatially resolved approach [15].

This research aims to highlight the great potential of the SR-μTXRD in the characterization of paint materials presenting high complexity in XRD phase analysis [24,25]. Such complexities are pervasive in CH investigations, where paint layers frequently exhibit a variety of challenging features, including (i) the presence of coexisting crystalline phases in the same layer, even in significantly different weight fractions; (ii) the occurrence of the same crystalline phases in contiguous layers; (iii) mixtures made by extremely fine crystallites co-existing with significantly coarser ones of the same species; and (iv) preferred orientation of crystallites. Therefore, this study presents the potential of synchrotron-based micro-X-ray diffraction in transmission geometry (SR-μTXRD) linear mapping to study the mineralogical composition, the layer sequence/thickness, and the microstructure of paint

layers (i.e., preferred orientation of pigments and fillers) in paint stratigraphies [8,15,26,27]. In recent years, growing attention has been devoted to the use of SR-μTXRD to characterize materials belonging to CH, and scientists have optimized the SR beamlines for their investigation by defining ad hoc setups, specific spatial resolutions, and detection limits. As reported by Smieska et al. [12], this has been facilitated by the establishment of new facilities, such as the MAX IV Laboratory in Lund, Sweden, and the modernization of existing European facilities. Notable examples include advancements at the European Synchrotron Radiation Facility (ESRF) in France, as well as planned upgrades at Elettra in Italy and SOLEIL in France.

The study is carried out on cross sections of mock-ups composed of five paint layers. One or two marker pigments and at least three inorganic fillers, characterized by different grain sizes (coarse grains and very fine grains in the mixture) and different spatial orientations (preferred orientation and/or random orientation in the 3D space), were used in a complex mixture in each paint layer. To validate the SR-μTXRD results, the mock-up specimens were preliminarily characterized through a multimethodological approach, employing home-laboratory analytical instruments.

The study highlights the capability of SR-μTXRD linear mapping to (i) explore, with a high spatial resolution, polycrystalline heterogeneous materials; (ii) provide high-quality data of multiphase systems having (or not having) a powder-like ideal configuration; and (iii) perform qualitative, quantitative, and a full-profile fit of the XRD patterns through the Rietveld method, even in the case of crystalline components with very low weight fraction.

2. Materials and Methods

2.1. Materials

Mock-up samples of paint stratigraphy were prepared ad hoc in our home laboratory, and their stratigraphy is reported in Table 1.

Table 1. Scheme of the paint stratigraphy: layer color composition (pigment and filler) and estimated expected thickness.

Paint Stratigraphy: Layer, Color, Composition, and Thickness				
Layer	**Color**	**Pigment**	**Fillers**	**Expected Thickness**
5	white	white lead	calcite, talc	60 μm
4	light blue	cobalt blue	calcite, talc	75 μm
3	red	hematite + Prussian blue	calcite, talc	75 μm
2	blue	azurite	wollastonite, portlandite	120 μm
1	white	titanium white	wollastonite, portlandite	105 μm
gypsum base				

Pigments and fillers used to prepare the mock-up were selected on the basis of the aforementioned research aims as well as on the following key points:

(i) the color palette of CH paint materials, embracing a wide range of pigments from different historical periods, including ancient mineral pigments (i.e., hematite), as well as more modern ones (Prussian blue, cobalt blue, titanium white) and inorganic fillers;
(ii) the need to select pigments/fillers characterized by an elemental marker, which has been used to unambiguously identify a specific paint layer; and
(iii) the need to prepare layers as homogeneous and reproducible as possible, which led us to select commercial materials and patented dispersants.

The substrate of paint stratigraphy samples was made of gypsum, obtained by mixing deionized water and calcium sulfate hemihydrate (bassanite, $CaSO_4 \cdot 1/2H_2O$), in a 1:2 = bassanite:water ratio. After the hydration of bassanite and the subsequent transformation into gypsum, the surface of the gypsum substrates was polished with an abrasive

paper of P800 mesh to obtain a flat surface to be painted. The paint stratigraphies were composed of 5 different layers, each of them characterized by a marker pigment (or mixture of pigments). The pigments selected for the study were "white lead" (mixture of cerussite $PbCO_3$ and hydrocerussite $Pb_3(CO_3)_2(OH)_2$), cobalt blue ($CoAl_2O_4$), hematite (Fe_2O_3), Prussian blue ($Fe_4[Fe(CN)_6]_3 \cdot H_2O$), azurite ($Cu_3(CO_3)_2(OH)_2$), and titanium white ($TiO_2$).

For the preparation of the paint layers, the pigments were finely ground before being used to make a concentrated colored paste [75% wt of the pigment was dispersed in 22.5% wt of water and 2.5% wt patented fillers, and a patented dispersant (AkzoNobel, Corporate Privacy Officer, Amsterdam, The Netherlands) was used to prevent pigment clumping]. Then, 62 mL of concentrated colored paste was dispersed in 200 mL of "white acrylic base" (AkzoNobel), containing calcite ($CaCO_3$) and talc ($Mg_3Si_4O_{10}(OH)_2$) as fillers/dispersants, and further diluted in water to reach the appropriate viscosity for their application on the substrate. Only the first-layer pigments were mixed using wollastonite ($CaSiO_3$) and portlandite ($Ca(OH)_2$) as fillers, due to the use of a pre-optimized paste for titanium white. The obtained paints were then applied, one by one, onto the gypsum surface with a brush. The mean thickness of each layer (hereafter reported as *expected thickness*) was determined *a priori* by overlapping a given number of coats of pigment film, which were estimated to be ~15 μm thick each by checking the thickness of dry single coats in cross sections under an optical microscope. The layer sequence and the detailed mineralogical composition of each layer are reported in Table 1. At complete drying, selected micro-fragments of the painted specimens were sampled and embedded in cold polymerizable epoxy resin. The embedded micro-fragment was then cut with a diamond-bladed circular saw and then lapped through a circular laboratory polisher on both sides to obtain a thin section of 700 μm thickness. The polishing stage enabled the thin section to be free of the surface resin layer and made it suitable to be analyzed in transmission mode.

2.2. Methods

A preliminary characterization of the investigated samples was performed in our home laboratory. Their features were first explored by optical microscopy in reflected light (OM) with a Leitz Ortholux microscope (magnifications in the range 11×–22×), coupled with a digital camera Nikon DS-5M/USB and managed by the Lucia Image ™ software (version 5.0). Backscattered (BSE) images were acquired by a JEOL 5910 LV scanning electron microscope (SEM) with a tungsten filament source, coupled with an energy dispersive X-ray spectrometer (EDS) IXRF-2000 (0–20 keV), to investigate the elemental composition and the textural features of the samples.

SR-μTXRD data were collected at the XRD1 beamline of the ELETTRA large-scale facility (Trieste, Italy). The investigations were performed on the mock-up samples, and the diffraction data were collected in the 2°–50° (2θ) angular range, using a focused monochromatic beam with λ = 0.701054 Å and a DECTRIS 2M single-photon counting detector (Figure 1).

Instrumental calibration for the synchrotron experiment was performed by using a standard LaB_6 (SRM from NIST, code 660c) polycrystalline sample in a borosilicate capillary (Ø 0.3 mm). The capillary was centered and rotated about the goniometer axis during X-ray exposure, with the rotation axis on the focal plane of the camera used for sample centering. The detector was kept in a fixed position during the different measurements, ensuring the same sample-detector distance and detector tilting.

For the mock-up samples, linear scans from the surface (layer 5) to the bulk (gypsum base) have been carried out with an elliptical beam of 30 × 15 μm^2 (horizontal × vertical), with a step size of 15 μm (vertical), which allowed proper probing of the different layers along the lane. The major axis (horizontal) of the beam has been set parallel to the layer sequence of the paint stratigraphy, while the minor axis (vertical) has been set perpendicular to the layer sequence, as schematically shown in Figure 2.

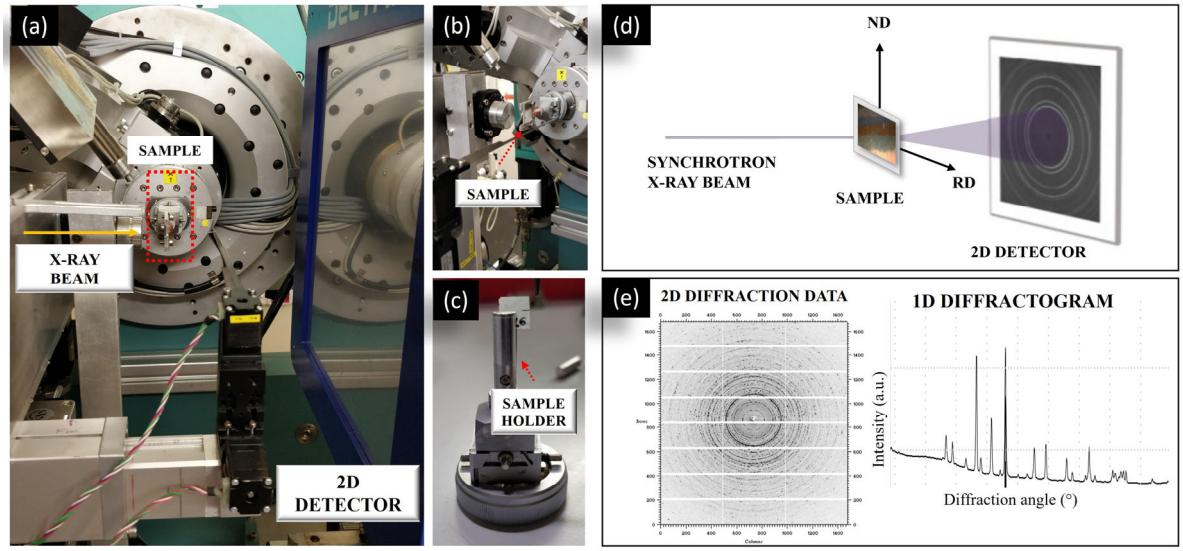

Figure 1. (**a**) Experimental set-up at the XRD1 beamline, ELETTRA Synchrotron Trieste; (**b**,**c**) paint stratigraphy sample on the sample holder; (**d**) schematic view of the experimental set-up; (**e**) 2D and 1D XRD pattern obtained using the Fit2D software.

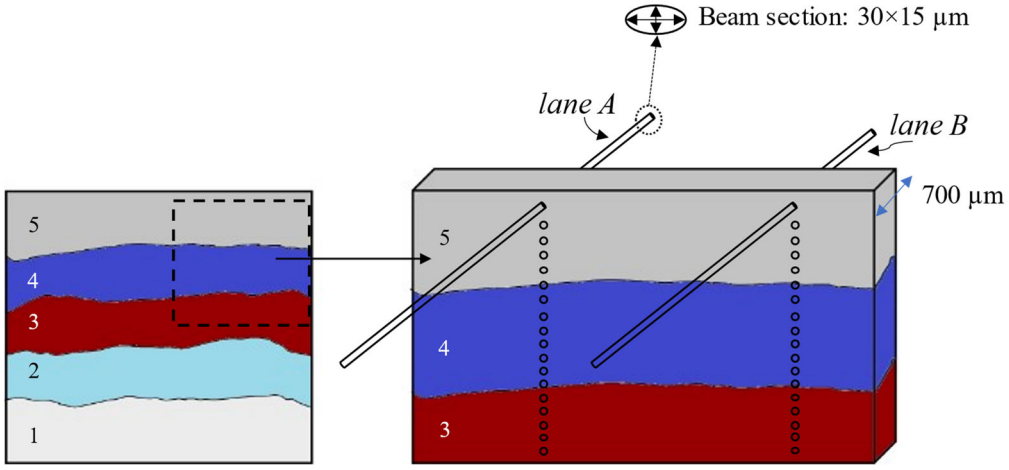

Figure 2. Schematic view of the paint stratigraphy layers and of the SR X-ray elliptical beam where the circles under the beam represent the sampling spots.

As a whole, 30 XRD diffraction patterns for each vertical scan were acquired, and the collections were repeated two times from different segments of the sample to obtain a good representation of the specimen. The exposure time was 60 s for each diffraction pattern. We evaluated the sample volume investigated per lane (~450 × 30 × 700 µm^3) as an adequate representation of the entire stratigraphy. The 2D XRD images were integrated by the Fit2D software V12.077 to generate the corresponding 1D diffraction patterns. A preliminary XRD qualitative phase analysis was performed using the PANalytical X'Pert High Score Plus 2.1.2 software, referring to the ICDD database (PDF-2). The SR-µTXRD patterns were then fitted by the Rietveld method using the GSAS-II package until convergence was achieved with final satisfactory values of the statistical parameters [26,27]. Data from the calibration experiment with LaB_6 were used to model the pseudo-Voigt peak profile function (as defined in GSAS-II) in order to reach the best full-profile fit of the collected patterns. Unit-cell parameters, average crystallite size, individual scale factor (for each crystalline species), zero shift, and a Chebychev polynomial function (used to model the background function) were refined during the Rietveld fit. Atomic coordinates and displacement parameters were not refined but used the data available in the literature. Preferred orientation correction

was applied to model only the profile function of talc [crystallographic plane (001)] and portlandite [plane (001)] by using the March–Dollase model [28]; the best fit was obtained with R_{MD} of *ca.* 0.81 and 0.85 for talc (001) and portlandite (001) peaks, respectively. When convergence was achieved, the statistical parameters suggested a good profile fit for all the diffraction patterns, having wR_p ranging between 7.4%–7.8% and GooF between 1.5–1.7.

3. Results and Discussion

This section describes the principal features of the paint stratigraphy (i.e., layer thickness, mineralogy, and microstructure), comparing the data obtained from home-laboratory analytical instruments to those from SR-μTXRD. Furthermore, a critical discussion of the results is provided, highlighting the limitations and/or potential of the analytical methods employed in this study.

3.1. Paint Stratigraphy: Layer Mineralogy

SEM-EDS analysis was used to acquire 2D maps of the paint stratigraphy, providing information about the chemical composition of the stratigraphy that allows us to reconstruct the type of pigments and filler in each single layer (Figure 3). For instance, the Cu elemental map unambiguously identifies layer 2, characterized by azurite (Figure 3c).

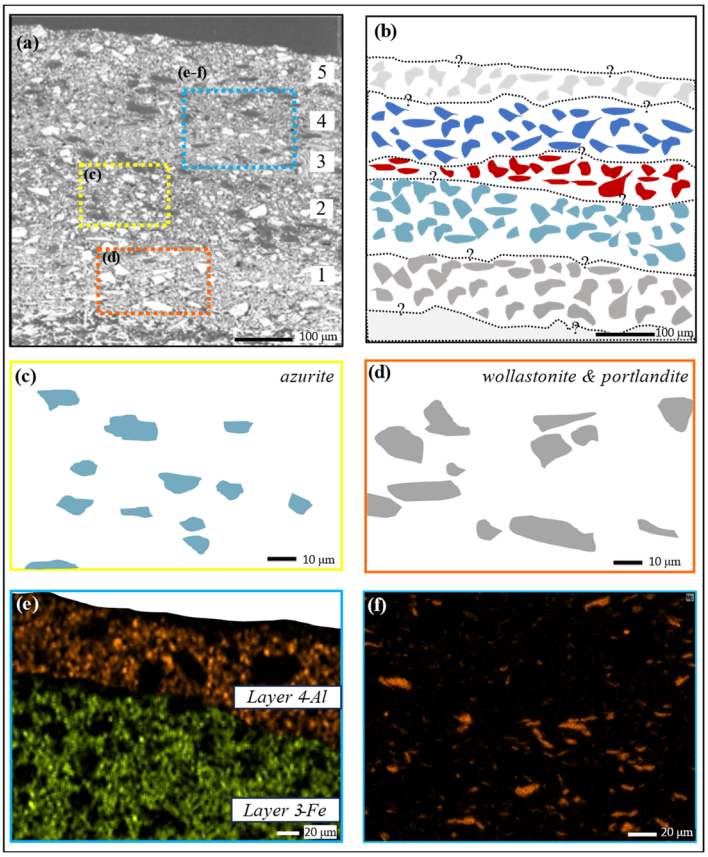

Figure 3. SEM-BSE images and EDS chemical maps: (**a**,**b**) stratigraphy image at 220× magnification and its schematic reconstruction (**b**); (**c**,**d**) magnification of pigment grain size in layers 2 (azurite) and 1 (wollastonite and portlandite); (**e**) Fe-Al chemical maps in layers 3–4 (hematite and Prussian blue and cobalt blue); (**f**) Mg chemical map in layers 3–4. Question marks have been added to the layer boundaries to indicate uncertainty in their identification. The five layers (1–5) are described in the text.

In some cases, the distribution maps of marker chemical elements failed in distinguishing some selected pigments from others, especially for those in a mixture that share

the same elemental marker, as in the case of hematite and Prussian blue in layer 3, both characterized by the dominant presence of iron (Figure 3e).

On the contrary, the thin sections investigated by SR-μTXRD enable the comprehensive mineralogical characterization of each single layer. In particular, this method provides a sequence of linear XRD mapping from the surface of the paint stratigraphy down to the core of the gypsum substrate, as described in Section 2.2. This analytical approach gave rise to a large number of XRD patterns, which contain a series of data discussed below. A total number of 30 patterns for each scan line have been collected and manually analyzed one by one. In Figure 4, a comparison among a selection of the most representative SR-μTXRD patterns, collected at different depths of the paint stratigraphy, is displayed.

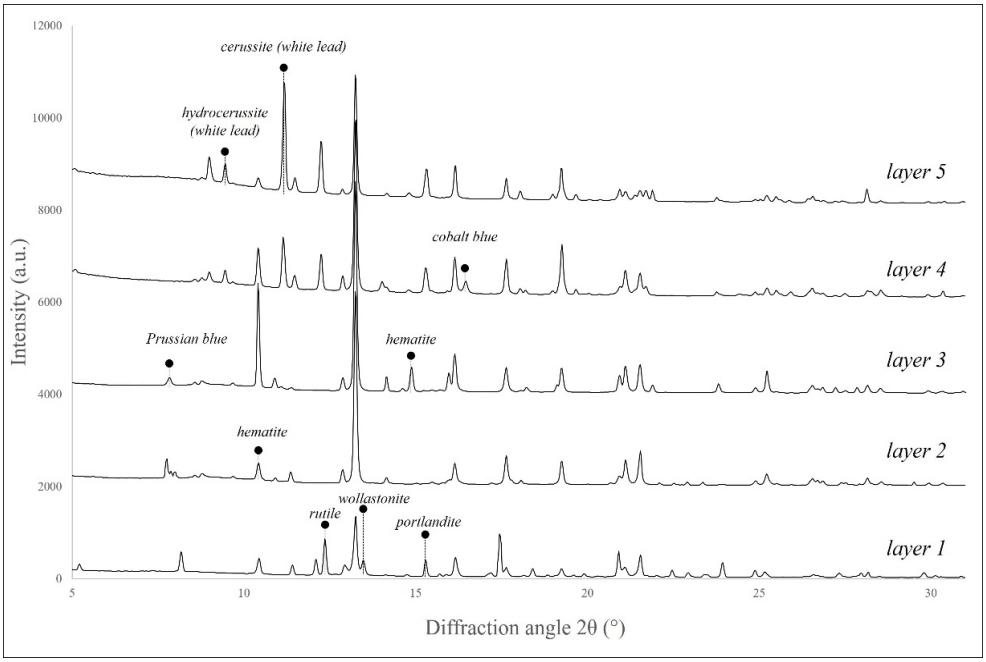

Figure 4. SR-μTXRD 1D patterns collected at different depths of the paint stratigraphy, representative for each one of the five layers.

The qualitative phase analysis showed that the crystalline components attributable to pigments (i.e., azurite, hematite, Prussian blue, cobalt blue, and white lead) and the filler fractions (i.e., calcite, talc, wollastonite) are easily distinguishable by their marker Bragg peaks. The qualitative phase analysis also revealed that (i) in the gypsum substrate, the presence of a low fraction of bassanite is most probably associated with its incomplete hydration into gypsum and (ii) in the wollastonite and portlandite layer, the occurrence of calcite is likely the result of a partial carbonation of portlandite during the setting, as we can see from the coating around the portlandite grains by SEM-EDS investigation.

Furthermore, the high brilliance of the synchrotron radiation, as well as the high signal-to-background ratio in the SR-μTXRD patterns, enabled the detection of the minor phases. For instance, the quantitative phase analysis carried out by the Rietveld method highlighted the coexistence of hematite and Prussian blue in low weight fraction (lower than 2% wt in the case of the Prussian Blue and lower than 7% wton average in the case of hematite).

3.2. Paint Stratigraphy: Layer Thickness

Figure 5a illustrates the thin section paint stratigraphy observed through reflected light microscopy, from which it was possible to investigate the thickness of each one of the five paint layers and to analyze the interface between juxtaposed layers (Figure 5b). By measuring the real thickness of each layer (based on 30 different segments for each layer), it was possible to estimate the average thickness for each of them, reported in Table 2 as

"*Optical thickness*". The mismatch between the "Optical thickness" and the expected one (SR-maximum estimated thickness) ended up being moderate, and, overall, they were in good agreement.

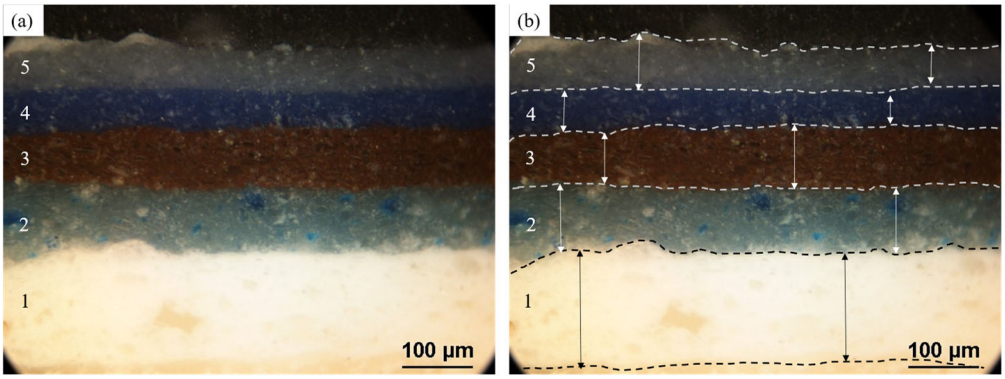

Figure 5. OM micrographs: (**a**) paint stratigraphy layers and (**b**) schematic reconstruction of the paint stratigraphy, where the arrows indicate some sampling segments used to calculate the average thickness. The five paint layers (1–5) are described in the text.

Table 2. Comparison between the expected thickness of each layer and the ones obtained by OM and SR-µTXRD.

Layer	Expected Thickness (µm)	Optical Thickness (µm)	OM St. Dev.	SR-µTXRD Maximum Thickness (µm)
5	60	60	10	105
4	75	50	10	105
3	75	70	10	120
2	120	90	10	90
1	105	150	20	165

The high standard deviation associated with the OM values (resulting in a variation higher than 10%) reflected a non-homogeneity of the layer thickness, which is also a common feature in paint stratigraphies of works of art.

BSE images failed in marking the boundary interface between contiguous layers. Layers 2–5 show all homogeneous grain size and contrast, making the different layers almost indistinguishable (Figure 3).

This is not the case with the SR-µTXRD analysis. The sequence of XRD data, from the surface of the paint stratigraphy down to the gypsum substrate (as described in Section 2.2), and the Rietveld fits of the diffraction patterns were used to develop a new way to provide the SR-maximum estimated thickness of paint layers. By tracking the presence and abundance of pigments (each of them a marker of one of the five paint layers) all through the paint stratigraphy, it is possible to obtain the thickness of each layer on the basis of its mineralogical composition. For instance, the thickness of the iron-bearing layer (layer 3) was measured to be ~75 µm by OM, while the presence of the iron-bearing pigment was identified to be at 120 µm to 225 µm depth from the paint surface. Remarkably, these measurements can be carried out on minor phases, proving the high potential of this SR-µTXRD approach in transmitting geometry to detect the occurrence in the depth of minor phases, with a microscale resolution and in relatively thick sections. The novelty of this innovative approach is that it opens new analytical routes for all those heterogeneous systems of cultural heritage, such as plasters and frescoes, for which preparation of thin sections by microtome (and without a glass slide support) is not always feasible (with, e.g., loss of grains and aggregates and formation of big holes) and the phase analysis (qualitative and quantitative) is fundamental. The calculated layer thickness of all the paint layers,

as obtained from the XRD full-profile fit, is given in Table 2. The values calculated from SR-μTXRD are in a good match with the estimated thickness from the optical investigations.

3.3. Paint Stratigraphy: Layer Microstructure

SEM-EDS analysis was performed to obtain data about the paint stratigraphy microstructure, i.e., pigment-filler grain size and spatial distribution of particles (Figure 3a–d).

In Figure 3, a schematization of SEM-EDS observations is reported, with a magnification of the different types of the grain size. In particular, the finer one in layer 2 refers to azurite (Figure 3c), while the coarser one in layer 1 refers to wollastonite and portlandite (Figure 3d). However, it was only possible to observe the differences between the grain size of the wollastonite and portlandite layer and the rest of the stratigraphy thanks to the coarser grain size and a higher brightness.

In addition, the chemical mapping helps to investigate another important element in the stratigraphy: the Mg contribution, coming from the unique phyllosilicate, is essential to reconstruct the preferred orientation of talc crystallites, arranged parallel to the layer surfaces due to the brushstroke movement (Figure 3f).

A further aspect that needs to be considered is that OM and SEM-EDS allow the characterization of an exposed surface, but the morphology and thickness of paint layers could be significantly different below the exposed surface due to the cross-section cutting and polishing. This condition is highly likely for thick sections, such as those of the present study, but it may occur even for very thin ones (like the ones obtained by microtome and having a 5–10 μm thickness). Hence, a bulk analysis able to investigate the volume below the exposed surface is highly desirable.

The analysis of 2D SR-μTXRD images allows additional and interesting considerations. In Figure 6, two 2D diffraction images collected at different depths are compared. Figure 6a refers to "ideal" XRD data collected from layer 5, where the Debye rings are well-defined, with constant intensity along the whole ring. This feature means that the crystalline phases that generate this XRD pattern have a micrometric grain size and are randomly oriented, which represents the condition of an ideal polycrystalline sample in the XRD experiments, a condition that also characterizes the SR-μTXRD layers 3 and 4. Consistently, the quality of the Rietveld full-profile fit, performed on the 1D diffraction pattern, is high (as suggested by the low wR_p values, <10%), and the phase fractions can be obtained without applying any threshold filter for overcoming the graininess problem (see below).

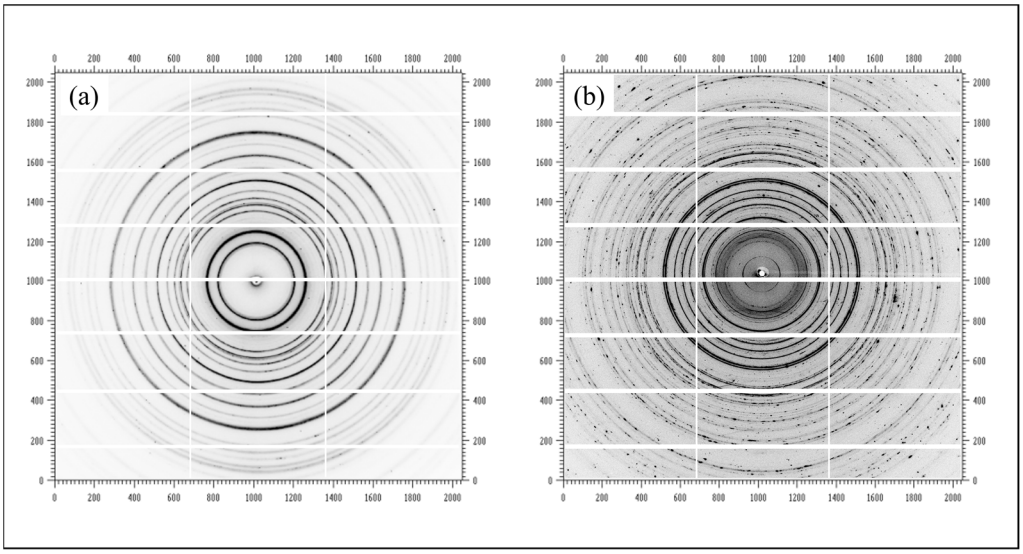

Figure 6. Diffraction patterns collected from different depths, with (**a**) an almost ideal Debye diffraction pattern and (**b**) affected by poor-particle statistics.

On the contrary, the two-dimensional diffraction image in Figure 6b was collected from the bulk of the sample and suggests that the investigated volume contains crystalline phases with different grain sizes, which generate inhomogeneous rings and uneven intensity with spots along the rings. Smooth diffraction rings, spotty rings, and intense isolated spots dominate the diffraction pattern. Despite the 2D image deviating significantly from the ideality, we performed the Rietveld profile fit of the 1D pattern, obtained from the azimuthal integration of the 2D XRD image, "*as it is*". Correcting the graininess issues would certainly have led to an improvement in the quality of the refinement. However, this would have precluded us from making further observations that were crucial for characterizing the paint stratigraphy (see below).

The average values of the weight fraction of marker crystalline phases (both pigments and fillers) are reported in Table 3, and the results of the Rietveld full-profile fit are shown in Figure 7. Crystalline phases of contiguous layers are included in the quantitative phase analysis, due to the XRD pattern acquired on the layer's interface (Table 3). As reported in Table 3, there is a low estimated standard deviation of the average weight fraction values, which suggests a homogeneous distribution of the crystalline phases within the investigated volume of each paint layer.

Table 3. Average weight fraction (%) of pigments and fillers, as obtained by the Rietveld full-profile fit. The estimated standard deviations are $\leq$ 0.1 % wt.

Layer—Pigment	Calcite	Talc	Hydro-Cerussite	Cerussite	Cobalt Blue	Hematite	Prussian Blue	Azurite	Wollastonite	Portlandite	Rutile
layer 5—white lead	75.2	7.4	13.3	4							
layer 4—cobalt blue	77.3	12.2	4.4	1.09	5						
layer 3—hematite + Prussian blue	83	7.1			2.2	6.9	2.0				
layer 2—azzurite	82.3	9.6						4.2	3.9	4.6	1.2
layer 1—Chalix titanium	58.4	7.6						3.7	12.2	11.8	14.6

A careful inspection of the XRD patterns offers a better understanding of the complexity of the microstructure of the paint stratigraphy. In Figure 8, the XRD patterns collected at different depths (i.e., 285 and 60 μm) are reported with an inset of the two diffraction peaks of calcite (d_{110} 2.50 Å and d_{202} 2.09 Å). For the lower layer (Figure 8a, at 285 μm depth), there is a good match between the calculated and observed profiles. Here, calcite does not occur in the form of large single crystals; it is rather micritic in size, as it is the result of the $Ca(OH)_2$ carbonation, a reaction that takes place when calcium hydroxide (portlandite) and carbon dioxide react, resulting in the formation of calcium carbonate ($Ca(OH)_2 + CO_2 \rightarrow CaCO_3 + H_2O$), which leads to the crystallization of calcite in the form of micro-crystals. On the contrary, in the upper layer (Figure 8b, at 60 μm depth), the significant difference between the calculated and observed profile, in terms of both intensity and peak shape, is attributable to the occurrence of large single crystals of calcite that belong to the filler fraction. SEM observations confirmed the absence of Ca-containing crystals (attributed to calcium carbonate of calcite) with grain size larger than 10 μm in the layer composed of wollastonite and portlandite (layer 1), showing the presence of Ca-bearing microcrystals (attributed to calcium carbonate of calcite, partially recrystallized) around the portlandite crystals.

The marked preferred orientation of the talc and portlandite platy crystallites, observed by SEM investigation, can also be extrapolated from the Rietveld full-profile fit. In all the XRD patterns, talc shows a marked orientation of the platy crystallites according to the (001) plane, which is strictly related to the way the pigmented pastes were laid down during the layering of paints. Therefore, to reach the best full-profile fit, it was necessary to correct the peak intensities for the preferred orientation effect. The same procedure was applied to the (001) diffraction planes for portlandite, which tend to have a platy habit as well.

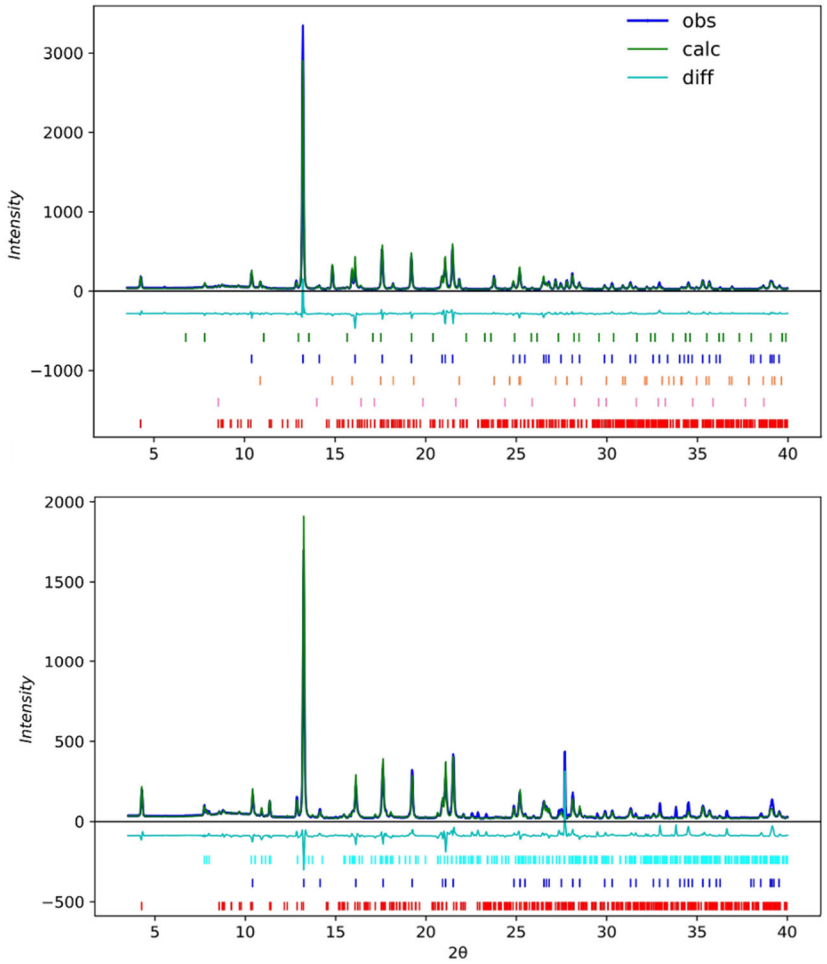

Figure 7. Two examples of the Rietveld full-profile fit pertaining to the SR-μTXRD patterns of layer 3 (**top**) and layer 2 (**bottom**). Color phase identification: green: Prussian blue; blue: calcite; orange: hematite; pink: spinel; red: talc; light blue: azurite.

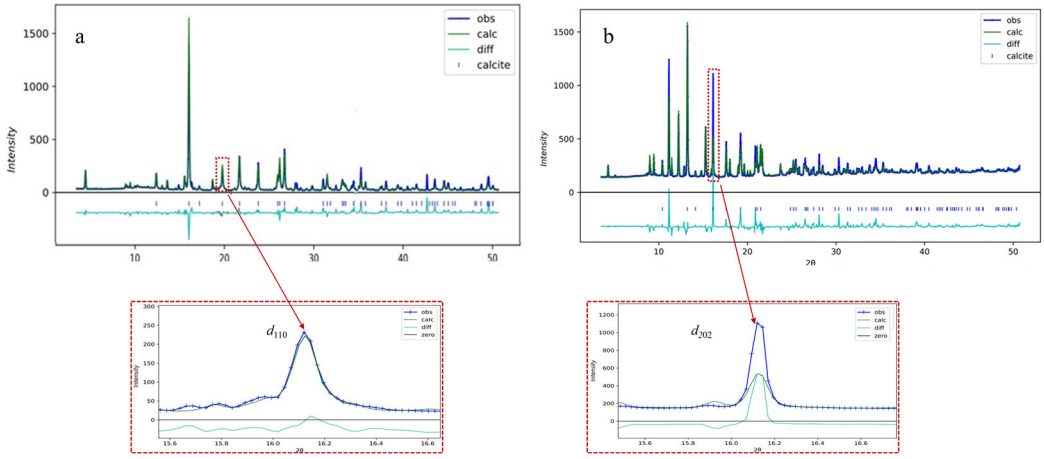

Figure 8. (**a**) XRD pattern collected at 285 μm depth with micritic calcite (layer 2); (**b**) pattern collected at 60 μm depth with large single crystals of calcite (layer 5). The magnification of two calcite peaks (d_{110} 2.50 Å and d_{202} 2.09 Å) is shown.

4. Conclusions

A new analytical approach combining SR XRD linear mapping and Rietveld full-profile fit to characterize the crystalline phases in a complex mixture in paint stratigraphies

is presented here. The investigations were carried out on mock-up stratigraphy to develop and validate a useful analytical procedure for the SR-μTXRD analysis. The mock-ups were prepared ad hoc to be characterized by a compositional and microstructural complexity: (i) a large number of paint layers; (ii) each layer composed of one or two marker pigments and at least three inorganic fillers; (iii) fillers and pigments characterized by different grain size (coarse grains and very fine grains in the mixture); and (iv) a different spatial orientation (preferred orientation and/or random orientation), as well as some crystalline phases in low weight fraction.

By performing a linear mapping of the stratigraphy with the SR X-ray beam, each one of the five paint layers of the stratigraphy was investigated.

This study proves that what may appear to be a criticality for a Rietveld full-profile fit can supply important information on CH materials, despite escaping the ideal conditions of powder diffraction (i.e., thousands of micrometric crystals randomly oriented in the sample volume). Following that, the advantages provided by the suggested approach also include the possibility (i) to identify the presence of a specific crystalline phase (for example, calcite) in different or contiguous paint layers and, at the same time, (ii) to demonstrate that the given phase has a different grain size or orientation in the different layers. This can aid in giving useful consideration to the manufacturing and grinding of the pigments, the painting technique (e.g., the influence of the brushstroke during the layering, as proven by the preferred orientation of crystallites, parallel to the layered surface), and the possible compositional phase changes occurring over time (e.g., the partial transformation of portlandite large crystals in micritic calcite ones). This approach can also help in distinguishing the primary calcite from the secondary one (recrystallization of calcite from calcium-containing solutions or by carbonatation) in multi-phase systems, where the discrimination of the origin of calcite is crucial, such as in the study of plasters, frescoes, and some archeological samples (e.g., pottery, ceramic fragments, bones).

The possibility to characterize oriented and/or large crystals, which give rise to single-crystal spots in 2D powder diffraction patterns, is also crucial to obtain novel information about those crystalline phases commonly occurring in paint stratigraphies (such as carbonate phases) that cannot be finely ground (such as azurite).

The drawbacks of the suggested procedure involve the need for micro-samples and the X-raying of the material. Hence, despite the SR-μTXRD analysis being non-destructive for the investigated sample, one should consider that a micro-sampling may not always be allowed for CH artworks and that compositional and microstructural changes may occur due to the high energy of SR X-rays, especially for metastable phases or organic components in the sample (such as organic binders).

Moreover, this study demonstrates that SR-μTXRD enables a deeper understanding of the mineralogy, microstructure, and configuration of the paint stratigraphy by using a single data set of XRD data without involving several complementary techniques.

Above all, our analytical approach enhances the potential of point-specific XRD methodologies, thus broadening analytical scenarios to a 2D investigation of multi-phase materials in CH, even in the absence of dedicated micro-mapping techniques. This high potential can be successfully applied not only to polychrome stratigraphies but also to other multi-layered systems, paving the way for new insights into the study of degradation processes and conservation procedures within CH materials.

Author Contributions: G.M., N.M., G.D.G. and E.P. wrote the main manuscript text. E.P., M.P. and G.B. performed the XRD analysis, and G.M., N.M. and E.P. interpreted the results, while M.C. helped with the Rietveld analysis. All authors (G.M., N.M., G.B., M.C., A.B., C.C., G.D.G., M.P., M.R. and E.P.) assisted with the revision of the initial draft of the manuscript. All authors have read and agreed to the published version of the manuscript.

Funding: Funding for this research was provided by the Italian Ministry of Education (MUR) through the projects "PRIN2017—Mineral reactivity, a key to understand large-scale processes: award No. 2017 L83S77" and "Dipartimenti di Eccellenza 2023–2027".

Data Availability Statement: Additional details pertaining to the Rietveld full-profile fits, described in this manuscript, can be obtained by the authors upon request.

Acknowledgments: The authors acknowledge the ELETTRA Synchrotron in Trieste (Italy) for the provision of synchrotron radiation facilities (CERIC-ERIC proposal nr. 20192094) and the Italian Ministry of Education (MUR). Three anonymous reviewers are warmly thanked for the revision of the manuscript.

Conflicts of Interest: The authors declare that they have no known competing financial interests or personal relationships that could have appeared to influence the work reported in this paper.

References

1. Janssens, K.; Alfeld, M.; Van der Snickt, G.; De Nolf, W.; Vanmeert, F.; Radepont, M.; Monico, L.; Dik, J.; Cotte, M.; Falkenberg, G.; et al. The Use of Synchrotron Radiation for the Characterization of Artists' Pigments and Paintings. *Ann. Rev. Anal. Chem.* **2013**, *6*, 399–425. [CrossRef] [PubMed]
2. Possenti, E.; Colombo, C.; Conti, C.; Gigli, L.; Merlini, M.; Plaisier, J.R.; Realini, M.; Gatta, D.G. What's underneath? A non-destructive depth profile of painted stratigraphies by synchrotron grazing incidence X-ray diffraction. *Analyst* **2018**, *143*, 4290. [CrossRef]
3. Vanmeert, F.; De Meyer, S.; Gestels, A.; Avranovich Clerici, E.; Deleu, N.; Legrand, S.; Van Espen, P.; Van der Snickt, G.; Alfeld, M.; Dik, J.; et al. Non-invasive and Non-destructive Examination of Artists' Pigments, Paints and Paintings by Means of X-ray Imaging Methods. In *Cultural Heritage Science*; Colombini, M.P., Degano, I., Nevin, A., Eds.; Springer: Cham, Switzerland, 2022.
4. Gonzalez, V.; Cotte, M.; Vanmeert, F.; De Nolf, W.; Janssens, K. X-ray Diffraction Mapping for Cultural Heritage Science: A Review of Experimental Configurations and Applications. *Chem.-Eur. J.* **2020**, *26*, 1703–1719. [CrossRef] [PubMed]
5. Janssens, K.; Van der Snickt, G.; Vanmeert, F.; Legrand, S.; Nuyts, G.; Alfred, M.; Monico, L.; Anaf, W.; De Nolf, W.; Vermeulen, M.; et al. Non-Invasive and Non-Destructive Examination of Artistic Pigments, Paints, and Paintings by Means of X-Ray Methods. *Top. Curr. Chem.* **2016**, *374*, 81. [CrossRef] [PubMed]
6. Dooryhée, E.; Anne, M.; Bardiés, I.; Hodeau, J.-L.; Martinetto, P.; Rondot, S.; Salomon, J.; Vaughan, G.B.M.; Walter, P. Non-destructive synchrotron X-ray diffraction mapping of a Roman painting. *Appl. Phys. A Mater. Sci. Process* **2005**, *81*, 663–667. [CrossRef]
7. Angelini, I.; Asscher, Y.; Secco, M.; Parisatto, M.; Artioli, G. The pigments of the frigidarium in the Sarno Baths, Pompeii: Identification, stratigraphy and weathering. *J. Cult. Herit.* **2019**, *40*, 309–316. [CrossRef]
8. Janssens, K.; Cotte, M. Using Synchrotron Radiation for Characterization of Cultural Heritage Materials. In *Synchrotron Light Sources and Free-Electron Lasers*; Jaeschke, E., Khan, S., Schneider, J., Hastings, J., Eds.; Springer: Cham, Switzerland, 2020. [CrossRef]
9. Cotte, M.; Dollman, K.; Fernandez, V.; Gonzalez, V.; Vanmeert, F.; Monico, L.; Dejoie, C.; Burghammer, M.; Huder, L.; Fisher, S.; et al. New Opportunities Offered by the ESRF to the Cultural and Natural Heritage Communities. *Synchrotron Radiat. News* **2022**, *35*, 3–9. [CrossRef]
10. Cotte, M.; Genty-Vincent, A.; Janssens, K.; Susini, J. Applications of Synchrotron X-ray Nano-Probes in the Field of Cultural Heritage. *C. R. Phys.* **2018**, *19*, 575–588. [CrossRef]
11. Possenti, E.; Colombo, C.; Conti, C.; Marinoni, N.; Merlini, M.; Negrotti, R.; Realini, M.; Gatta, G.D. Consolidation of building materials with a phosphate-based treatment: Effects on the microstructure and on the 3D pore network. *Mater. Charact.* **2019**, *54*, 315–329. [CrossRef]
12. Smieska, L.M.; Woll, A.R.; Vanmeert, F.; Janssens, K. Synchrotron-Based High-Energy X-ray MA-XRF and MA-XRD for Art and Archaeology. *Synchrotron Radiat. News* **2019**, *32*, 29–33.
13. Gianoncelli, A.; Schoder, S.; Plaisier, J.R.; Fugazzotto, M.; VBarone, G.; Russo, A.; Mazzoleni, P.; Raneri, S. X-ray Synchrotron Radiation to Look at Pigments in Antiquities: Overview and Examples. *Heritage* **2024**, *7*, 2118–2137. [CrossRef]
14. Cotte, M.; Gonzalez, V.; Vanmeert, F.; Monico, L.; Dejoie, C.; Burghammer, M.; Huder, L.; De Nolf, W.; Fisher, S.; Fazlic, I.; et al. The "Historical Materials BAG": A New Facilitated Access to Synchrotron X-ray Diffraction Analyses for Cultural Heritage Materials at the European Synchrotron Radiation Facility. *Molecules* **2022**, *27*, 1997. [CrossRef] [PubMed]
15. Bertrand, L.; Cotte, M.; Stampanoni, M.; Thoury, M.; Marone, F.; Schöder, S. Development and trends in synchrotron studies of ancient and historical materials. *Phys. Rep.* **2012**, *519*, 51–96. [CrossRef]
16. Østergaard, J.S. Polychromy, sculptural, Greek and Roman. In *The Oxford Classical Dictionary*; Oxford University Press: Oxford, UK, 2018. [CrossRef]
17. Pouyet, E.; Fayard, B.; Salomé, M.; Taniguchi, Y.; Sette, F.; Cotte, M. Thin-sections of painting fragments: Opportunities for combined synchrotron-based micro-spectroscopic techniques. *Herit. Sci.* **2015**, *3*, 3. [CrossRef]
18. Ghirardello, M.; Gonzalez, V.; Monico, L.; Nevin, A.; MacLennan, D.; Schmidt Patterson, C.; Burghammer, M.; Réfrégiers, M.; Comelli, D.; Cotte, M. Application of Synchrotron Radiation-Based Micro-Analysis on Cadmium Yellows in Pablo Picasso's Femme. *Microsc. Microanal.* **2022**, *28*, 1504–1513. [CrossRef] [PubMed]
19. Dal Fovo, A.; Martínez-Weinbaum, M.; Oujja, M.; Castillejo, M.; Fontana, R. Reflectance Spectroscopy as a Novel Tool for Thickness Measurements of Paint Layers. *Molecules* **2023**, *28*, 4683. [CrossRef] [PubMed]

20. Possenti, E.; Conti, C.; Gatta, G.D.; Merlini, M.; Realini, M.; Colombo, C. Synchrotron radiation μ X-ray diffraction in transmission geometry for investigating the penetration depth of conservation treatments on cultural heritage stone materials. *Anal. Methods* **2020**, *12*, 1587–1594. [CrossRef]
21. Švarcová, S.; Bezdička, P.; Hradil, D.; Hradilová, J.; Žižak, I. Clay Pigment Structure Characterisation as a Guide for Provenance Determination—A Comparison between Laboratory Powder Micro-XRD and Synchrotron Radiation XRD. *Anal. Bioanal. Chem.* **2011**, *399*, 331–336. [CrossRef]
22. Gonzalez, V.; van Loon, A.; Price, S.W.T.; Noble, P.; Keune, K. Synchrotron micro-XRD and micro-XRD-CT reveal newly formed lead–sulfur compounds in Old Master paintings. *J. Anal. At. Spectrom.* **2020**, *35*, 2267–2273. [CrossRef]
23. Massinelli, G.; Marinoni, N.; Colombo, C.; Gatta, G.D.; Realini, M.; Burghammer, M.; Possenti, E. Advanced mapping of inorganic treatments on porous carbonate stones by combined synchrotron radiation high lateral μXRPD and μXRF. *Sci. Rep.* **2024**, *14*, 9108. [CrossRef]
24. Howard, H.; Najorka, J.; Schofield, P.F.; Geraki, K. Degradation of Fourteenth-century Mordant Gilding Layers: Synchrotron-based Microfocus XRF, XRD, and XANES Analyses of Two Paintings by Pietro Lorenzetti. *Stud. Conserv.* **2023**, *69*, 193–208. [CrossRef]
25. Hiley, C.I.; Hansford, G.; Eastaugh, N. High-resolution non-invasive X-ray diffraction analysis of artists' paints. *J. Cult. Herit.* **2022**, *53*, 1–13. [CrossRef]
26. Toby, B.H.; Von Dreele, R.B. GSAS-II: The genesis of a modern open-source all purpose crystallography software package. *J. Appl. Cryst.* **2013**, *46*, 544–549. [CrossRef]
27. McCusker, L.B.; Von Dreele, R.B.; Cox, D.E.; Louer, D.; Scardi, P. Rietveld refinement guidelines. *J. Appl. Cryst.* **1999**, *32*, 36–50. [CrossRef]
28. Dollase, W.A. Correction of Intensities for Preferred Orientation in Powder Diffractometry: Application of the March Model. *J. Appl. Cryst.* **1986**, *19*, 267–272. [CrossRef]